ACS APPLIED NANO MATERIALS

www.acsanm.org Article

# Bacterial Production of Barley Stripe Mosaic Virus Biotemplates for Palladium Nanoparticle Growth

Yu-Hsuan Lee,[#] Kok Zhi Lee,[#] Rachel G. Susler, Corren A. Scott, Longfei Wang, L. Sue Loesch-Fries, Michael T. Harris, and Kevin V. Solomon*

Cite This: https://dx.doi.org/10.1021/acsanm.0c02570 Read Online

ACCESS | Metrics & More | Article Recommendations | Supporting Information

**ABSTRACT:** Barley stripe mosaic virus (BSMV) has recently been proposed as an attractive biotemplate for direct metallic nanomaterial synthesis as it interacts with metal precursors through multiple mechanisms. These interactions more than double the coating capacity for metal and accelerate nanomaterial synthesis, reducing costs, while potentially offering economical synthesis pathways for a wider range of nanomaterials. However, these studies were only able to generate BSMV via plant production, which is not well suited to widescale industrial production and limits engineering of BSMV-templated material properties to protein mutations that maintain or enhance infectivity in plants. Here, BSMV virus-like particles (VLPs) are produced from bacteria for the first time by fusing the origin of assembly from tobacco mosaic virus (TMV) to the transcript encoding BSMV capsid protein. Purification of BSMV-VLPs produced from *Escherichia coli* results in nanorods that average 82 nm in length and 21 nm in diameter. We also demonstrate that these rod-shaped BSMV-VLPs can be more rapidly coated with Pd metal than *in planta*-produced BSMV in the absence of an external reducing agent. This study creates an alternate platform for BSMV-VLP production and enables future engineering opportunities to tune nanomaterial properties through biotemplate design.

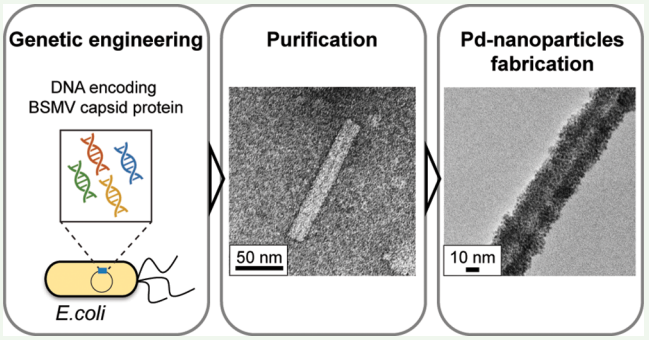


**KEYWORDS:** *biotemplate, barley stripe mosaic virus (BSMV), VLP, synthetic biology, E. coli, protein expression*



## INTRODUCTION

Bottom-up nanofabrication via templating on naturally occurring biomolecules (biotemplating) is a promising strategy for nanomaterial synthesis, as the products are frequently more uniform and less polydisperse.[1−8] For biotemplates such as plant virus capsid proteins, biotemplate structure is encoded within the protein primary sequence, which enables spontaneous self-assembly of hierarchical complex nanomaterials for diverse applications.[9−11] These scaffolds present diverse biochemical functionalities on their surface for interaction and coating with various metals. Plant tobacco mosaic virus (TMV) capsid proteins have been utilized as biotemplates and coated with metals such as Ag,[6] Pd,[12−15] Pt,[16] and Au,[12] and Au/Pd alloys[17] for incorporation in devices as battery electrodes,[18,19] memory devices,[20] catalysts,[3] and chemical sensors.[21]

Given the versatility of TMV, alternative biotemplates based on related viruses from the Virgaviridae family have been proposed. These alternatives present novel surface functionalities that provide new opportunities for the fabrication of nanoscaled materials. In particular, we have established that *in planta* produced barley stripe mosaic virus (BSMV) from the Virgaviridae family is an exciting alternate template for the synthesis of palladium nanorods.[22] The synthesized nanorods have similar properties to TMV such as morphology and a high adsorption capacity for palladium species. However, unlike TMV, BSMV-mediated reduction and deposition of metal precursor ions proceeds via a multistep Langmuir isotherm that incorporates both electrostatic and covalently driven affinity of metal precursor molecules for amino acid residues on the BSMV surface.[22] These electrostatic interactions have the potential to diversify the metals that may be deposited on template, which can be coated more quickly than TMV, leading to more economical processing for a given metal density.

Current approaches to produce BSMV are limited to *in planta* production, which makes its development challenging. First, modification to the genomes of *in planta*-synthesized viruses that may enhance biotemplating functionality may not

**Received:** September 24, 2020
**Accepted:** November 17, 2020




https://dx.doi.org/10.1021/acsanm.0c02570
ACS Appl. Nano Mater. XXXX, XXX, XXX−XXX

be stable, as these modifications may not confer a selective advantage for viral propogation.[23] Second, as these viruses are plant pathogens, virus-producing plants must be grown in specialized facilities to prevent infection of plants in the wild.[24] Finally, the viral replication cycle in plants requires 2−3 weeks, which results in slow, long, and complicated processes to extract relatively small amounts of viral capsids. On the other hand, alternative production processes that use bacterial expression platforms are faster and simpler.[25−27] Bacteria grow rapidly within 24 h in fermenters, which have been developed and optimized for decades for use in the food, beverage, biopharma, and biotech sectors. Bacterial hosts can also produce virus-like particles (VLPs) of assembled viral capsid proteins at higher yields and at shorter times when compared to other hosts, including yeast, baculovirus-insect cells, mammalian cells, and plants. Moreover, the use of a heterologous host reduces the evolutionary pressures on virus replication, enabling more opportunities for favorable genetical engineering of VLP structure. For example, TMV capsid protein (CP) has been modified to present on its surface a thiol group from cysteine, an amine group from lysine, or carboxylate groups from glutamate and aspartate, enabling chemical modification of the template at precise locations via covalent coupling,[28−30] conjugation,[31−34] and click chemistry.[35] Thiol introduction on TMV surfaces also enables deposition of diverse metals, including Au,[12,18] Ni,[18] Co,[18] and Pd.[4,12−15,36,37] These engineered modifications can be introduced easily and frequently do not compromise VLP structures while enhancing functionality.[38,39]

As members of Virgaviridae, both TMV and BSMV CPs self-assemble into long nanorod-shaped structures through protein−protein and protein−nucleic acid interactions (Figures 1 and 2). CPs initially self-assemble into disk-like

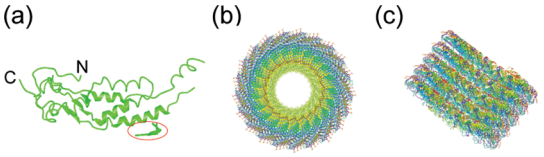


**Figure 1.** BSMV capsid protein and its assembly as a nanorod (a) BSMV capsid protein. N- and C-termini are labeled as N and C, respectively. The amino acids that interact with BSMV RNA are circled. Current crystal structures are only partial but capture ~90% of all residues. (b) Top-down view of assembled BSMV capsid proteins. (c) Side view of an assembled BSMV virion. The highest resolution crystal structure (PDB:5A7A[42]) was obtained from NCBI MMDB database[43] and rendered using Cn3D.[44]

structures via several protein−protein interactions. Nanorod assembly is then initiated via interactions of these CP disks with an RNA stem-loop structure called an origin of assembly sequence (OAS).[40,41] Upon binding of the OAS with the disk interior, the initial nucleating CP disk shifts conformation to a right-hand helix. This conformational shift also restructures the encapsulated RNA transcript to allow for rapid CP polymerization in a helical pattern around the RNA transcript to form a nanorod. Interactions of adjacent CPs in this nanorod are stabilized via a cluster of charged residues called the Casper carboxylate center.[42]

BSMV-VLPs have not been produced in a bacterial host to date, as a native OAS to initiate its assembly remains unidentified. However, chimeric BSMV viral particles have been shown to form due to interactions between BSMV CPs

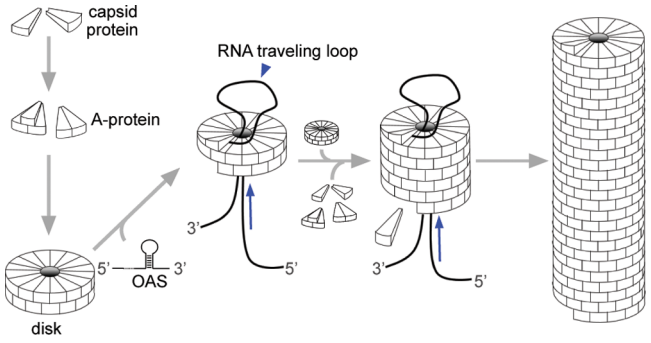


**Figure 2.** Assembly process of TMV involves multiple molecular interactions. Interactions between capsid proteins form "A-protein" and subsequently a disk structure before the origin of assembly sequence (OAS) on an RNA transcript initiates virus assembly. Subsequent disks and capsid proteins are assembled into a virus rod via protein−protein interaction and protein−RNA interaction.

and the TMV genome[41,42] in plants. Thus, we evaluated whether the TMV OAS may be sufficient to initiate BSMV-VLP assembly in bacteria. The introduced OAS successfully enabled assembly of BSMV CPs into rod-shaped VLPs in *E. coli*. After optimization of the expression, purification, and processing conditions, we produced BSMV-VLPs that could be used as biotemplates for synthesis of palladium-coated nanorods via hydrothermal processing. This bacterial synthesis platform for BSMV-VLP readily accelerates the production of BSMV-templated nanomaterials and opens new opportunities to tune nanomaterial properties via template engineering.

## RESULTS AND DISCUSSION

The self-assembly of BSMV-VLP relies on interactions between virus RNA and CPs, and interactions between adjacent capsid protein subunits (Figure 2). As the TMV OAS is recognized by BSMV-CP in plants,[41,42] we hypothesized that BSMV-CP transcripts with a TMV OAS at the 3′ end can initiate VLP assembly via RNA−CP interactions and lead to the formation of BSMV-VLPs (Figure 3). BSMV CP expression plasmids, which were codon-optimized for bacterial expression, were designed with and without a TMV OAS. BSMV-CP was initially expressed at 37 °C for 4 h in

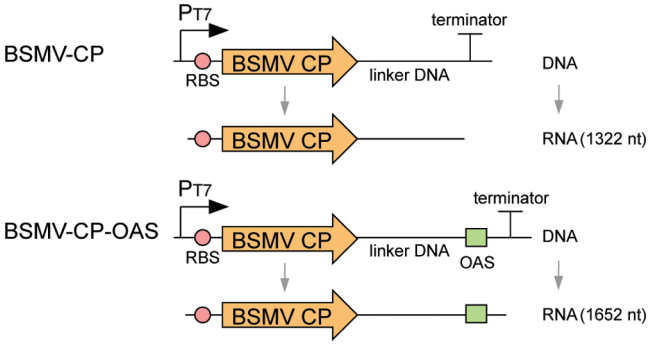


**Figure 3.** BSMV capsid protein expression constructs. Transcripts made from BSMV-CP (top) contain the BSMV-CP ORF and a linker RNA for a total length of 1322 nt. Transcripts made from BSMV-CP-OAS are similar, but they contain an OAS following the linker for a total length of 1652 nt (bottom). Both gene cassettes are driven by T7 promoter ($P_{T7}$), induced by IPTG, and translation is initiated via the native ribosomal binding site (RBS) of the parent expression vector.


https://dx.doi.org/10.1021/acsanm.0c02570
ACS Appl. Nano Mater. XXXX, XXX, XXX−XXX

*Escherichia coli* before lysing. Crude protein lysate was then centrifuged through several rounds to purify any synthesized VLPs, which were then characterized using transmission electron microscopy (TEM). TEM images did not show any BSMV rod-shaped VLPs or disk structures (data not shown) suggesting that BSMV CPs were not produced, did not self-assemble or that the isolation procedure was insufficient to capture produced VLPs. TMV constructs were expressed and purified as a positive control. Subsequent electron microscopy displayed the presence of TMV-VLPs, excluding the possibility of inefficient VLP isolation. Moreover, disk-shaped structures will form if wild-type CPs are successfully expressed in the host but fail to self-assemble into rod VLPs.[45] Thus, the absence of BSMV disk structures suggested poor soluble CP expression. To examine expression, crude protein lysates from *E. coli* with induced CP plasmids were analyzed via SDS-PAGE (Figure 4). SDS-PAGE analysis revealed a relatively heavy band of BSMV protein in the bacterial insoluble pellet suggesting that the majority of the CPs was misfolded (Figure 4a).

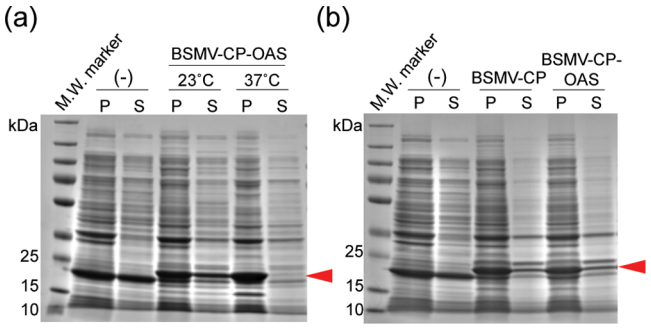


**Figure 4.** Expression of BSMV-CP-OAS at reduced temperatures leads to VLPs. (a) SDS-PAGE analysis of BSMV capsid protein (BSMV-CP-OAS) expression at room temperature (23 °C) and 37 °C, respectively. P represents the pellet and S represents the supernatant after centrifugation at 92,000 × g for 20 min. (b) SDS-PAGE analysis of cultures expressing BSMV-CP, BSMV-CP-OAS or a negative control lacking expression plasmid at room temperature. Arrows indicate the BSMV capsid protein at ~22.5 kDa.

Heterologous proteins, such as BSMV CP, may misfold at high temperatures due to too rapid protein synthesis and increased hydrophobic interactions that lead to the formation of insoluble protein aggregates in inclusion bodies.[46,47] To address this, we lowered the expression temperature to room temperature and extended the expression time from 4 to 16 h in order to slow down the protein expression rate and facilitate proper protein folding.[47] SDS-PAGE analysis revealed that reducing the expression temperature significantly increased soluble CP expression (Figure 4a). TEM analysis showed that the BSMV-CP-OAS construct did indeed form rod-shaped BSMV-VLPs while only disk structures formed from the OAS-free construct (Figure 5). SDS-PAGE confirmed soluble capsid protein expression under these conditions for both BSMV-CP and BSMV-CP-OAS constructs (Figure 4). Thus, the TMV OAS is sufficient for BSMV-VLP assembly in bacteria, which is consistent with previous studies *in planta*[42] (Figure 5 and Figure S1A). In the absence of an OAS, only disks formed (Figure 5a).

To increase the yield of soluble BSMV CP, we further optimized protein expression. As the inducer concentration affects the rate of protein expression and subsequent folding, we hypothesized that reduced IPTG concentrations would induce expression of more soluble protein. We tested IPTG concentrations of 0.10, 0.075, 0.050, and 0.010 mM and assessed the expression of BSMV CPs in the soluble fraction by SDS-PAGE. As shown in Figure 6, 0.075 and 0.10 mM IPTG induced higher yields of soluble CP, which is consistent with microbial expression of other VLPs such as TMV1Cys expression in *E. coli*.[45]

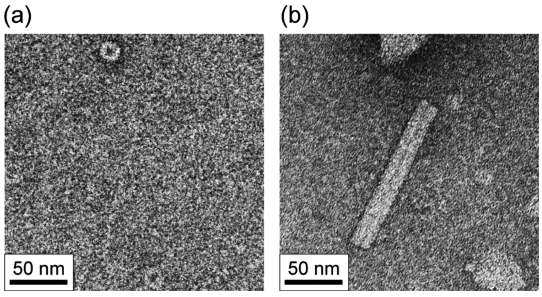


**Figure 5.** TEM analysis of VLPs assembled in vivo from BSMV-CP translated from an RNA (a) without an OAS and (b) with an OAS. Scale bar: 50 nm.

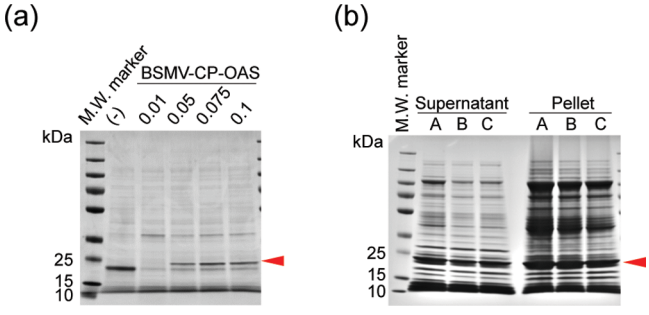


**Figure 6.** Analysis of BSMV-CP expression and solubilization. (a) SDS-PAGE analysis of BSMV-CP-OAS in 5 $\mu$g of bacterial preparations induced by different concentrations of IPTG (0.01, 0.05, 0.075, and 0.10 mM) compared with a negative control strain lacking the BSMV-CP-OAS expression plasmid. (b) SDS-PAGE analysis of the solubility of BSMV-CP-OAS in selected buffers: A. water, B Tris buffer, C sodium phosphate buffer. Arrows indicate BSMV capsid protein at ~22.5 kDa.

The buffer used to solubilize the final VLP product had a significant impact on the yield of VLPs. Sodium phosphate buffer ($Na_2HPO_4$, 10 mM, pH 7) is often used to solubilize VLPs, but its use here led to the formation of a white precipitate of aggregated VLPs over time (data not shown). That is, BSMV-VLPs were not stable in solution with $Na_2HPO_4$ and may have coagulated due to counterion adsorption neutralizing the electrostatic interactions of the BSMV surface.[48,49] Therefore, we investigated water and 10 mM tris(hydroxymethyl)aminomethane (Tris−HCl), pH 7, as resuspension buffers, which form ions with weaker net charge and/or different geometries that may interact more weakly. Although, BSMV-VLPs appeared to be equally soluble in water, or Tris or phosphate buffers (Figure 6b), there was no precipitation in Tris or water over time. However, due to the pH buffering, Tris buffer was used in all subsequent preparations.

To isolate VLPs for characterization, the preparations were centrifuged at 64,000 × g for 1 h over a saturated sucrose cushion.[21] However, BSMV-VLPs of various lengths were distributed throughout the sucrose cushion as shown in Figure


https://dx.doi.org/10.1021/acsanm.0c02570
ACS Appl. Nano Mater. XXXX, XXX, XXX−XXX

7 a and b. The BSMV-VLPs were often found in end-to-end (linear) and side-by-side (raft) aggregates (Figure 7). End-to-

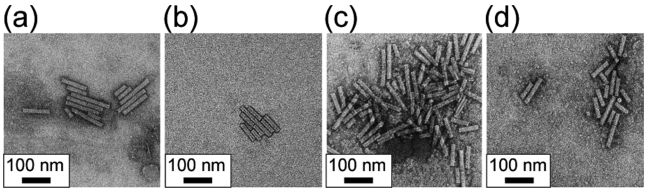


**Figure 7.** Analysis of BSMV-CP-OAS VLPs following centrifugation at 64,000 × g for 1 h over a saturated sucrose cushion. (a) VLPs isolated above the cushion; (b) VLPs at the bottom of the cushion. (c, d) VLPs without centrifugation through sucrose cushion. Scale bar: 100 nm.

end aggregates have been observed in some preparations of BSMV replicated *in planta*, which were linear aggregates of up to 40 viral particles.[50] Similarly, raft aggregates are common drying artifacts of TEM preparations;[51] in both cases, aggregate can arise due to the interfacial forces that arise during sample drying and staining for TEM visualization,[52] and thus sample preparation needs optimization. Because the VLPs did not form homogeneous bands in sucrose (Figure 7a,b), cushions were not used for purification (Figure 7c,d).

The purified BSMV-VLPs analyzed by TEM were nanorods that ranged in size from 20 to 160 nm in length with an average of 82 nm (Figure 8). These nanorods had a measured

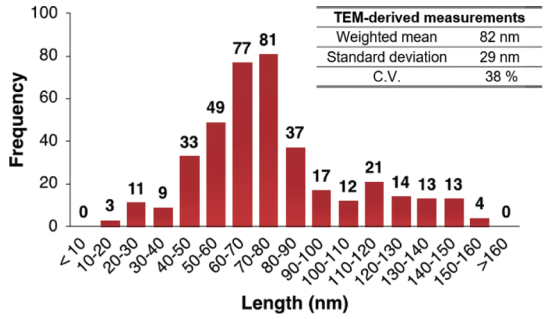


**Figure 8.** Length distribution histogram of BSMV-VLPs.

diameter of 21 nm. BSMV viral particle length is typically a function of the size of the encapsidated RNA, which initiates self-assembly.[53] In related TMV, the length of the encapsidated OAS-containing transcript directly scales with VLP size, serving as a molecular ruler.[54] Assuming a similar scaling to wild-type BSMV, one would expect our VLP constructs to attain a size of ~1 nm/27 nt or ~ 61 nm. The observed lengths were more than 30% higher than expected and could be a result of the nonnative TMV OAS creating novel secondary interactions that expanded the structure of the encapsidated RNA and the resulting viral particle or uncontrolled assembly beyond the molecular ruler. To determine the heterogeneity or purity of the VLP preparations, the size distribution was measured by dynamic light scattering (DLS) (Table 1). DLS measures the hydrodynamic radius, or size of an equivalent particle that diffuses with the same rate, and is a rough estimate of particle size that is distinct from its physical dimensions for nonspherical particles. The hydrodynamic radius of rod-like VLPs is at least half the radius of gyration,[55,56] a geometrical property calculated from the measured physical dimenstions.[56] Using our TEM-measured dimensions, we estimate that the

**Table 1. Length of VLPs as Measured by Dynamic Light Scattering (DLS)**

| size (hydrodynamic diameter) (nm) | relative abundance (%) | standard deviation (nm) | coefficient of variation (%) |
|---|---|---|---|
| 476.5 | 92.3 | 157.7 | 33 |
| 38.0 | 7.7 | 6.4 | 17 |

VLPs have a radius of gyration of 9.4−47 nm or a hydrodynamic radius of at least 4.7−23 nm. Analysis of the VLP preparation yielded a bimodal distribution of hydrodynamic radii with peaks at 38.0 nm (8%) and 476.5 nm (92%) (Table 1). The majority of the DLS-measured particles (476.5 nm) are two-orders of magnitude larger than expected VLP particles suggesting that the purified VLP exists primarily in aggregates as observed by TEM or complexed with other cellular impurities. The smaller peak is consistent with linear aggregates of BSMV, which are commonly observed in the literature.[50] While future work is needed to optimize the purification of individual VLP particles, *E. coli* produced BSMV-VLPs display similar architecture to wild-type viral particles.

The BSMV-VLPs were coated with palladium via a hydrothermal process to evaluate their capability as a biotemplate for nanomaterial synthesis. The BSMV-VLPs were coated in the absence of an external reducing agent by incubation in a stirred reaction vessel with 0.75 mM $Na_2PdCl_4$ precursor solution. As shown in Figure 9 and Figure S1B,

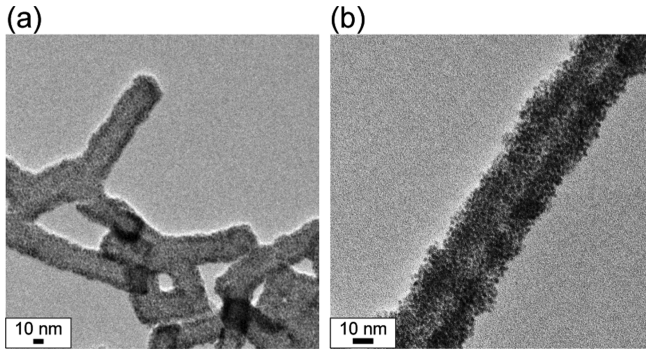


**Figure 9.** TEM image of a palladium-coated BMSV-VLP nanorod. Scale bar: 10 nm.

BSMV-VLPs were successfully coated with a layer of palladium nanoparticles in a single round of processing. The Pd layer is dense and fully coated, increasing the nanomaterial diameter to 33 nm (~12 nm thick coating). Multiple coating cycles are typically required to achieve similar properties in *in planta*-produced TMV and BSMV. Similar single layer coatings with *in planta*-produced TMV[12,36] are nonuniform and only up to ~7 nm thick. Plant-generated BSMV,[22] on the other hand, was observed to require two rounds of processing to achieve similar coating thicknesses with Pd; however, this study conducted its metal deposition at 55 °C rather than the 57 °C tested here. The results indicate BSMV-VLPs produced from *E. coli* can serve as effective biotemplates for nanomaterial synthesis, achieving similar or better coating thicknesses in fewer processing steps than current production platforms.


https://dx.doi.org/10.1021/acsanm.0c02570
ACS Appl. Nano Mater. XXXX, XXX, XXX−XXX

**Table 2. Strains and Plasmids**

| name | relevant genotype | vector backbone | plasmid origin | source |
|---|---|---|---|---|
| **strains** | | | | |
| BL21-CodonPlus(DE3)-RIPL | *E. coli* B F$^-$ *ompT hsdS*($r_B^-$ $m_B^-$) *dcm*$^+$ Tet$^r$ *gal* $\lambda$(DE3) *endA* Hte [*argU proL* Cam$^r$] [*argU ileY leuW* Strep/Spec$^r$] | N/A | N/A | Agilent Technologies, Santa Clara, CA |
| **plasmids** | | | | |
| pET21-BSMV-CP-linker-OAS | BMSV-CP-linker-OAS, *bla* | pET21-1cys-tmv-cp (original backbone: pET-21a(+))[41] | pBR322 | this study |
| pET21-BSMV-CP-linker | BMSV-CP-linker, *bla* | pET21-1cys-tmv-cp (original backbone: pET-21a(+) )[41] | pBR322 | this study |

## CONCLUSIONS

In summary, we have developed techniques for the production of novel BSMV-VLPs from a bacterial expression system. The expression of BSMV-VLPs was achieved by fusing an OAS sequence from TMV downstream of mRNA encoding BSMV CP. *E. coli* production platforms offer unique opportunities for genetic engineering and faster protein expression; therefore, the development of our system enables rapid design-build-test cycles for the engineering and production of BSMV-VLPs with desired properties. VLP expression was optimized by controlling expression temperature and isolation buffers used during purification, resulting in effective cell lysis and higher yields of soluble BSMV CP. The BSMV-VLPs were also shown to be effective biotemplates for the synthesis of inorganic nanomaterials of high quality. This work enables the generation of BSMV-derived biotemplates that expand the toolbox for bottom-up nanomaterial synthesis.

## METHODS

**Cloning of BSMV Capsid Protein Expression Plasmid.** *E. coli* strains and plasmids used in this study are listed in Table 2. All molecular biology manipulations were carried out according to standard practices.[57] A codon-optimized DNA sequence containing BSMV capsid protein cDNA, linker DNA[54] and TMV OAS cDNA (BSMV-CP-linker-OAS) was synthesized by IDT (Coralville, IA) (Supporting Information). This sequence was first ligated to the pGEM-T-Easy intermediate vector (Promega, Madison, WI; Cat. No.: A1360) before cloning into the vector pET21-1cys-tmv-cp (provided by Professor Culver, University of Maryland, College Park) between the *NdeI* and *XhoI* restriction sites, generating pET21-BSMV-CP-linker-OAS. pET21-BSMV-CP-linker-OAS was subsequently digested with *SalI* and *XhoI* to remove the OAS, blunt-ended with Klenow fragment (NEB, Ipswich, MA; Cat. No.: M0210S), and religated to itself, generating pET21-BSMV-CP-linker. All constructs were sequence verified via Sanger sequencing at Genewiz (South Plainfield, NJ).

**BSMV Capsid Protein Expression Conditions.** The BSMV CP expression plasmids were transformed into *E. coli* BL21-CodonPlus (DE3)-RIPL (Agilent Technologies, Santa Clara, CA; Cat. No.: #230280). The bacteria were streaked onto plates containing LB media plus 100 $\mu$g/mL ampicillin and 25 $\mu$g/ml chloramphenicol and incubated for 16−20 h at 37 °C. Single colonies were selected, inoculated into LB broth, and incubated at 37 °C for 16−20 h at 250 rpm. The liquid cultures were then diluted 100-fold in LB broth and incubated at 37 °C until an $OD_{600}$ of 0.5. The cultures were induced with the addition of 0.1 mM isopropyl $\beta$-D-1-thiogalactopyranoside (IPTG) for expression of the BSMV CP followed by incubation for 16−20 h at room temperature (~23 °C) to express CP. All BL21-CodonPlus (DE3)-RIPL liquid cultures or plates contained ampicillin (100 $\mu$g/ml) and chloramphenicol (25 $\mu$g/ml). Bacteria were collected by centrifugation at room temperature for 5 min at 6000 rpm. The pellet containing the bacteria was used directly for isolation of BSMV-VLPs or stored at −80 °C.

**BSMV-VLP Purification.** BSMV-VLPs were isolated from *E. coli* by resuspension in Bugbuster protein isolation solution (MilliporeSigma, Burlington, MA) according to the manufacturer's instructions, supplemented with 1.2 mM dithiothreitol. Lysonase Bioprocessing Reagent (MilliporeSigma, Burlington, MA) was added according per the manufacturer's instructions and the suspension was incubated for 10 min at room temperature to lyse the cells followed by centrifugation at 19,000 × g for 10 min to remove insoluble debris. The VLPs in the preparation were isolated by centrifugation at 64,000 × g at 4 °C for 1 h followed by resuspension in 10 mM Tris−HCl, pH 7.

In an attempt to remove large aggregates from the VLP suspension, preparations were layered over a saturated sucrose cushion and spun at 19,000 × g for 10 min at room temperature in an Optima TL Ultracentrifuge (Beckman Coulter, Brea, CA). A top light-scattering band in the cushion was collected and centrifuged at 64,000 × g at 4 °C for 1 h and resuspended in 0.01 M Tris−HCl buffer at pH 7. For samples purified without a sucrose cushion, the lysate supernatant was centrifuged at 19,000 × g for 10 min at room temperature. The supernatant was collected and centrifuged at 64,000 × g at 4 °C for 1 h. The resulting pellet containing the VLPs was resuspended in 0.01 M Tris−HCl buffer at pH 7.

**Verification of Coat Protein Expression.** To validate coat protein expression, cell lysates were analyzed on 4−20% polyacrylamide gels (Thermo Fisher Scientific, Waltham, MA; Cat. No.: XP04200BOX). Fourteen microliters of protein lysate was mixed with an equal volume of 2X Tris-glycine SDS Sample Buffer (Thermo Fisher Scientific, Waltham, MA; Cat. No.: LC2676) and supplemented with 2 $\mu$L of 1 M DTT (Thermo Fisher Scientific, Waltham, MA; Cat. No.: AC426380100). Samples were then incubated at 85 °C for 5 min to denature the proteins. Samples were then placed on ice for 5 min before being loaded on to the gel. PageRuler Plus Prestained Protein Ladder (Thermo Fisher Scientific, Waltham, MA; Cat. No.: 26620) was used as a molecular weight standard. The gels were run at 120 V for an hour before staining with Coomassie blue (Fisher Scientific, Pittsburgh, PA; Cat. No.: BP101−25) for 10 min. Gels were then destained with destaining buffer (10% glacial acetic acid and 10% methanol) overnight before visualization under visible light with an Azure c400 imager (Azure Biosystems, Dublin, CA).

**TEM Imaging.** Samples were prepared for imaging in a 200 kV Tecnai T20 TEM by placing 1.5 $\mu$l of the VLP suspension onto formvar/carbon coated copper grids followed by an equal amount of ACS-grade phosphotungstic acid (PTA, stock concentration: 1%) for negative staining. After 15 s, the excess liquid was wicked from the grid with 3MM paper and the grid was allowed to dry. At least 50 images were taken per sample using a calibrated Gatan Ultrascan 1000 CCD camera (Gatan Inc., Pleasanton, CA). More than 20 images with good contrast and focus were analyzed with the ImageJ software to measure the dimensions of ~400 nanorods.

**Size Measurement by Dynamic Light Scattering.** The refractive index of purified BSMV-VLPs was measured in 0.01 M Tris buffer (pH 7) by an ABBE-3L refractometer (Thermo Fisher Scientific, Waltham, MA). The obtained VLP refractive index (1.3551) with the refractive index of the Tris resuspension buffer (1.3500) and viscosity (1.00037 cP)[58] were used for subsequent


https://dx.doi.org/10.1021/acsanm.0c02570
ACS Appl. Nano Mater. XXXX, XXX, XXX−XXX

dynamic light-scattering detection with a scattering angle of 17° by a Malvern Zetasizer Nano ZS (Malvern Panalytical Ltd., UK).

**Metal Coating Process.** Metal coating of the VLPs was performed in a 100 mL CSTR reactor vessel at 57 °C. The VLPs and 0.75 mM ACS-grade sodium tetrachloropalladate (II) ($Na_2PdCl_4$) (Sigma Aldrich, St Louis, MO) were added to the reaction vessel for 20 min and stirred continuously. The coated biotemplate aggregates spontaneously precipitated and were washed repeatedly with distilled, deionized water (18 MΩ) to remove residual salt and precursor solution.

## ■ ASSOCIATED CONTENT

### Supporting Information

The Supporting Information is available free of charge at https://pubs.acs.org/doi/10.1021/acsanm.0c02570.

DNA sequence of synthesized BSMV-CP-linker-OAS construct

SEM images of uncoated and coated BSMV-VLPs (PDF)

## ■ AUTHOR INFORMATION


### Corresponding Author

**Kevin V. Solomon** − *225 South University Street, Agricultural & Biological Engineering, 1203 West State Street, Bindley Bioscience Center, and 500 Central Drive, Laboratory of Renewable Resources Engineering (LORRE), Purdue University, West Lafayette, Indiana 47907-2093, United States;* orcid.org/0000-0003-2904-9118; Email: kvs@purdue.edu

### Authors

**Yu-Hsuan Lee** − *School of Chemical Engineering, Purdue University, West Lafayette, Indiana 47907, United States*

**Kok Zhi Lee** − *225 South University Street, Agricultural & Biological Engineering and 1203 West State Street, Bindley Bioscience Center, Purdue University, West Lafayette, Indiana 47907-2093, United States*

**Rachel G. Susler** − *School of Chemical Engineering, Purdue University, West Lafayette, Indiana 47907, United States*

**Corren A. Scott** − *School of Chemical Engineering, Purdue University, West Lafayette, Indiana 47907, United States*

**Longfei Wang** − *915 West State Street, Department of Botany and Plant Pathology, Purdue University, West Lafayette, Indiana 47907, United States*

**L. Sue Loesch-Fries** − *915 West State Street, Department of Botany and Plant Pathology, Purdue University, West Lafayette, Indiana 47907, United States*

**Michael T. Harris** − *School of Chemical Engineering, Purdue University, West Lafayette, Indiana 47907, United States;* orcid.org/0000-0002-0797-8701

Complete contact information is available at: https://pubs.acs.org/10.1021/acsanm.0c02570

### Author Contributions

#Y.-H. L. and K.Z.L. contributed equally.


### Notes

The authors declare no competing financial interest.

## ■ ACKNOWLEDGMENTS

We would like to gratefully thank Dr. James Culver at the University of Maryland Biotechnology Institute, Center for Biosystems Research, for his insights on the production of VLPs. This material is based upon work supported by the National Science Foundation under Grant No. CBET-2028618. The research was also supported by the Robert B. and Virginia V. Covalt Professorship of Chemical Engineering, the Purdue Department of Botany & Plant Pathology, the Purdue Research Foundation (Fellowships #60000025 and #60000029), the USDA National Institute of Food and Agriculture (Hatch Multistate Project S1075) and startup funds from the Purdue Colleges of Agriculture and Engineering. Electron microscopy was performed with the help of Dr. Christopher J. Gilpin, Laurie Mueller, and Robert Seiler in the Purdue Life Science Microscopy Facility.

## ■ REFERENCES


(1) Flynn, C. E.; Lee, S.-W.; Peelle, B. R.; Belcher, A. M. Viruses as vehicles for growth organization and assembly of materials. *Acta Mater.* **2003**, *51*, 5867−5880.

(2) Knez, M.; Sumser, M.; Bittner, A. M.; Wege, C.; Jeske, H.; Martin, T. P.; Kern, K. Spatially selective nucleation of metal clusters on the tobacco mosaic virus. *Adv. Funct. Mater.* **2004**, *14*, 116−124.

(3) Yang, C.; Manocchi, A. K.; Lee, B.; Yi, H. Viral-templated palladium nanocatalysts for Suzuki coupling reaction. *J. Mater. Chem.* **2011**, *21*, 187−194.

(4) Manocchi, A. K.; Horelik, N. E.; Lee, B.; Yi, H. Simple, readily controllable palladium nanoparticle formation on surface-assembled viral nanotemplates. *Langmuir* **2010**, *26*, 3670−3677.

(5) Dujardin, E.; Peet, C.; Stubbs, G.; Culver, J. N.; Mann, S. Organization of metallic nanoparticles using tobacco mosaic virus templates. *Nano Lett.* **2003**, *3*, 413−417.

(6) Lee, S.-Y.; Royston, E.; Culver, J. N.; Harris, M. T. Improved Metal Cluster Deposition on a Genetically Engineered Tobacco Mosaic Virus Template. *Nanotechnology* **2005**, *16*, S435−S441.

(7) Zhang, Y.; Dong, Y.; Zhou, J.; Li, X.; Wang, F. Application of plant viruses as a biotemplate for nanomaterial fabrication. *Molecules* **2018**, *23*, 2311.

(8) Kim, I.; Kang, K.; Oh, M. H.; Yang, M. Y.; Park, I.; Nam, Y. S. Virus-Templated Self-Mineralization of Ligand-Free Colloidal Palladium Nanostructures for High Surface Activity and Stability. *Adv. Funct. Mater.* **2017**, *27*, 1703262.

(9) Jeevanandam, J.; Pal, K.; Danquah, M. K. Virus-like nanoparticles as a novel delivery tool in gene therapy. *Biochimie* **2019**, *157*, 38−47.

(10) Chu, S.; Brown, A. D.; Culver, J. N.; Ghodssi, R. Tobacco Mosaic Virus as a Versatile Platform for Molecular Assembly and Device Fabrication. *Biotechnol. J.* **2018**, *13*, 1800147.

(11) Larkin, E. J.; Brown, A. D.; Culver, J. N., Fabrication of tobacco mosaic virus-like nanorods for peptide display. In *Virus-Derived Nanoparticles for Advanced Technologies*, Springer: 2018; pp. 51−60.

(12) Lim, J.-S.; Kim, S.-M.; Lee, S.-Y.; Stach, E. A.; Culver, J. N.; Harris, M. T. Quantitative Study of Au(III) and Pd(II) Ion Biosorption on Genetically Engineered Tobacco Mosaic Virus. *J. Colloid Interface Sci.* **2010**, *342*, 455−461.

(13) Freer, A. S.; Guarnaccio, L.; Wafford, K.; Smith, J.; Steilberg, J.; Culver, J. N.; Harris, M. T. SAXS characterization of genetically engineered tobacco mosaic virus nanorods coated with palladium in the absence of external reducing agents. *J. Colloid Interface Sci.* **2013**, *392*, 213−218.

(14) Adigun, O. O.; Freer, A. S.; Miller, J. T.; Loesch-Fries, L. S.; Kim, B. S.; Harris, M. T. Mechanistic Study of the Hydrothermal Reduction of Palladium on the Tobacco Mosaic Virus. *J. Colloid Interface Sci.* **2015**, *450*, 1−6.

(15) Adigun, O. O.; Novikova, G.; Retzlaff-Roberts, E. L.; Kim, B.; Miller, J. T.; Loesch-Fries, L. S.; Harris, M. T. Decoupling and elucidation of surface-driven processes during inorganic mineralization on virus templates. *J. Colloid Interface Sci.* **2016**, *483*, 165−176.

(16) Lee, S.-Y.; Choi, J.; Royston, E.; Janes, D. B.; Culver, J. N.; Harris, M. T. Deposition of Platinum Clusters on Surface-Modified Tobacco Mosaic Virus. *J. Nanosci. Nanotechnol.* **2006**, *6*, 974−981.

(17) Lim, J.-S.; Kim, S.-M.; Lee, S.-Y.; Stach, E. A.; Culver, J. N.; Harris, M. T. Formation of au/pd alloy nanoparticles on TMV. *J. Nanomaterials* **2010**, *2010*, 1−6.
(18) Royston, E.; Ghosh, A.; Kofinas, P.; Harris, M. T.; Culver, J. N. Self-assembly of virus-structured high surface area nanomaterials and their application as battery electrodes. *Langmuir* **2008**, *24*, 906−912.
(19) Chen, X.; Gerasopoulos, K.; Guo, J.; Brown, A.; Wang, C.; Ghodssi, R.; Culver, J. N. Virus-Enabled Silicon Anode for Lithium-Ion Batteries. *ACS Nano* **2010**, *4*, 5366−5372.
(20) Tseng, R. J.; Tsai, C.; Ma, L.; Ouyang, J.; Ozkan, C. S.; Yang, Y. Digital memory device based on tobacco mosaic virus conjugated with nanoparticles. *Nat. Nanotechnol.* **2006**, *1*, 72.
(21) Bruckman, M. A.; Liu, J.; Koley, G.; Li, Y.; Benicewicz, B.; Niu, Z.; Wang, Q. Tobacco mosaic virus based thin film sensor for detection of volatile organic compounds. *J. Mater. Chem.* **2010**, *20*, 5715−5719.
(22) Adigun, O. O.; Retzlaff-Roberts, E. L.; Novikova, G.; Wang, L.; Kim, B.-S.; Ilavsky, J.; Miller, J. T.; Loesch-Fries, L. S.; Harris, M. T. BSMV as a biotemplate for palladium nanomaterial synthesis. *Langmuir* **2017**, *33*, 1716−1724.
(23) Yusibov, V.; Shivprasad, S.; Turpen, T.; Dawson, W.; Koprowski, H., Plant viral vectors based on tobamoviruses. In *Plant Biotechnology*, Springer: 2000; pp. 81−94.
(24) Brewer, H. C.; Hird, D. L.; Bailey, A. M.; Seal, S. E.; Foster, G. D. A guide to the contained use of plant virus infectious clones. *Plant biotechnol. J.* **2018**, *16*, 832−843.
(25) Jeong, H.; Seong, B. L. Exploiting virus-like particles as innovative vaccines against emerging viral infections. *J. Microbiology* **2017**, *55*, 220−230.
(26) Zeltins, A. Construction and characterization of virus-like particles: a review. *Mol. Biotechnol.* **2013**, *53*, 92−107.
(27) Schneemann, A.; Young, M. J. Viral assembly using heterologous expression systems and cell extracts. *Adv. Protein Chem.* **2003**, *64*, 1−36.
(28) Meunier, S.; Strable, E.; Finn, M. Crosslinking of and coupling to viral capsid proteins by tyrosine oxidation. *Chem. Biol.* **2004**, *11*, 319−326.
(29) Pokorski, J. K.; Steinmetz, N. F. The art of engineering viral nanoparticles. *Mol. Pharmaceutics* **2010**, *8*, 29−43.
(30) Aljabali, A. A.; Barclay, J. E.; Butt, J. N.; Lomonossoff, G. P.; Evans, D. J. Redox-active ferrocene-modified Cowpea mosaic virus nanoparticles. *Dalton Trans.* **2010**, *39*, 7569−7574.
(31) Molino, N. M.; Wang, S.-W. Caged protein nanoparticles for drug delivery. *Curr. Opin. Biotechnol.* **2014**, *28*, 75−82.
(32) Wen, A. M.; Shukla, S.; Saxena, P.; Aljabali, A. A.; Yildiz, I.; Dey, S.; Mealy, J. E.; Yang, A. C.; Evans, D. J.; Lomonossoff, G. P. Interior engineering of a viral nanoparticle and its tumor homing properties. *Biomacromolecules* **2012**, *13*, 3990−4001.
(33) Zhou, K.; Li, F.; Dai, G.; Meng, C.; Wang, Q. Disulfide bond: dramatically enhanced assembly capability and structural stability of tobacco mosaic virus nanorods. *Biomacromolecules* **2013**, *14*, 2593−2600.
(34) Zhou, K.; Zhang, J.; Wang, Q. Site-Selective Nucleation and Controlled Growth of Gold Nanostructures in Tobacco Mosaic Virus Nanotubulars. *Small* **2015**, *11*, 2505−2509.
(35) Bruckman, M. A.; Kaur, G.; Lee, L. A.; Xie, F.; Sepulveda, J.; Breitenkamp, R.; Zhang, X.; Joralemon, M.; Russell, T. P.; Emrick, T. Surface modification of tobacco mosaic virus with "click" chemistry. *ChemBioChem* **2008**, *9*, 519−523.
(36) Lim, J.-S.; Kim, S.-M.; Lee, S.-Y.; Stach, E. A.; Culver, J. N.; Harris, M. T. Biotemplated aqueous-phase palladium crystallization in the absence of external reducing agents. *Nano Lett.* **2010**, *10*, 3863−3867.
(37) Lee, S. Y.; Lim, J. S.; Harris, M. T. Synthesis and application of virus-based hybrid nanomaterials. *Biotechnol. Bioeng.* **2012**, *109*, 16−30.
(38) Yi, H.; Nisar, S.; Lee, S.-Y.; Powers, M. A.; Bentley, W. E.; Payne, G. F.; Ghodssi, R.; Rubloff, G. W.; Harris, M. T.; Culver, J. N. Patterned assembly of genetically modified viral nanotemplates via nucleic acid hybridization. *Nano Lett.* **2005**, *5*, 1931−1936.
(39) Geiger, F. C.; Eber, F. J.; Eiben, S.; Mueller, A.; Jeske, H.; Spatz, J. P.; Wege, C. TMV nanorods with programmed longitudinal domains of differently addressable coat proteins. *Nanoscale* **2013**, *5*, 3808−3816.
(40) Butler, P. J. G. The current picture of the structure and assembly of tobacco mosaic virus. *J. Gen. Virol.* **1984**, *65*, 253−279.
(41) Butler, P. Self−assembly of tobacco mosaic virus: the role of an intermediate aggregate in generating both specificity and speed. *Philos. Trans. R. Soc. London, Ser. B* **1999**, *354*, 537−550.
(42) Clare, D. K.; Pechnikova, E. V.; Skurat, E. V.; Makarov, V. V.; Sokolova, O. S.; Solovyev, A. G.; Orlova, E. V. Novel inter-subunit contacts in barley stripe mosaic virus revealed by cryo-electron microscopy. *Structure* **2015**, *23*, 1815−1826.
(43) Madej, T.; Lanczycki, C. J.; Zhang, D.; Thiessen, P. A.; Geer, R. C.; Marchler-Bauer, A.; Bryant, S. H. MMDB and VAST+: tracking structural similarities between macromolecular complexes. *Nucleic Acids Res.* **2013**, *42*, D297−D303.
(44) Wang, Y.; Geer, L. Y.; Chappey, C.; Kans, J. A.; Bryant, S. H. Cn3D: sequence and structure views for Entrez. *Trends Biochem. Sci.* **2000**, *25*, 300−302.
(45) Brown, A. D.; Naves, L.; Wang, X.; Ghodssi, R.; Culver, J. N. Carboxylate-directed in vivo assembly of virus-like nanorods and tubes for the display of functional peptides and residues. *Biomacromolecules* **2013**, *14*, 3123−3129.
(46) Villaverde, A.; Carrió, M. M. Protein aggregation in recombinant bacteria: biological role of inclusion bodies. *Biotechnol. Lett.* **2003**, *25*, 1385−1395.
(47) Sørensen, H. P.; Mortensen, K. K. Soluble expression of recombinant proteins in the cytoplasm of Escherichia coli. *Microb. cell fac.* **2005**, *4*, 1.
(48) Donovan, A. R.; Adams, C. D.; Ma, Y.; Stephan, C.; Eichholz, T.; Shi, H. Fate of nanoparticles during alum and ferric coagulation monitored using single particle ICP-MS. *Chemosphere* **2018**, *195*, 531−541.
(49) Xu, C.-Y.; Xu, R.-K.; Li, J.-Y.; Deng, K.-Y. Phosphate-induced aggregation kinetics of hematite and goethite nanoparticles. *J. Soils and Sed.* **2017**, *17*, 352−363.
(50) Kassanis, B.; Slykhuis, J. Some properties of barley stripe mosaic virus. *Ann. of Appl. Biol.* **1959**, *47*, 254−263.
(51) Michen, B.; Geers, C.; Vanhecke, D.; Endes, C.; Rothen-Rutishauser, B.; Balog, S.; Petri-Fink, A. Avoiding drying-artifacts in transmission electron microscopy: Characterizing the size and colloidal state of nanoparticles. *Sci. Rep.* **2015**, *5*, 9793.
(52) Israelachvili, J. N., *Intermolecular and Surface Forces*. Academic Press: 2011; 704.
(53) Chiko, A. W. Evidence of multiple virion components in leaf-dip preparations of barley stripe mosaic virus. *Virology* **1975**, *63*, 115−122.
(54) Saunders, K.; Lomonossoff, G. P. In planta synthesis of designer-length tobacco mosaic virus-based nano-rods that can be used to fabricate nano-wires. *Front. in plant sci.* **2017**, *8*, 1335.
(55) Burchard, W., Static and dynamic light scattering approaches to structure determination of biopolymers. In *Laser light scattering in biochemistry*, Harding, S. E.; Sattelle, D. B.; Bloomfield, V. A., Eds. Royal Society of Chemis: Cambridge, 1992; 3−22.
(56) Santos, N. C.; Castanho, M. A. Teaching light scattering spectroscopy: the dimension and shape of tobacco mosaic virus. *Biophys. J.* **1996**, *71*, 1641−1650.
(57) Green, M. R., *Molecular Cloning: A Laboratory Manual*. Cold Spring Harbor Laboratory 2012.
(58) Chairatana, P.; Chu, H.; Castillo, P. A.; Shen, B.; Bevins, C. L.; Nolan, E. M. Proteolysis triggers self-assembly and unmasks innate immune function of a human α-defensin peptide. *Chem. Sci.* **2016**, *7*, 1738−1752.


https://dx.doi.org/10.1021/acsanm.0c02570
*ACS Appl. Nano Mater.* XXXX, XXX, XXX−XXX